The 8th European Congress on Computational Methods in Applied Sciences and Engineering
ECCOMAS Congress 2022
5–9 June 2022, Oslo, Norway

SIMULATION OF THE FLOW-ACOUSTIC-STRUCTURAL INTERACTION IN FLOW DUCTS USING A PARTITIONED APPROACH IN THE TIME DOMAIN

Jurgen Kersschot[1,2], Hervé Denayer[1,2], Wim De Roeck[1] and Wim Desmet[1,2]

[1] Department of Mechanical Engineering, KU Leuven, Belgium, jurgen.kersschot@kuleuven.be

[2] DMMS Core Lab, Flanders Make, Belgium

Key words: Partitioned simulation approach, Flow-acoustic-structural interaction

Abstract. Duct systems confining a subsonic air flow, such as ventilation ducts, often have a lightweight design. These lightweight constructions are easily excited by unsteady pressure fluctuations in the flow, causing structural vibrations and noise emissions. Designing effective solutions for this flow-acoustic-structural problem requires a better understanding of the multi-physical interactions and efficient prediction tools. In this work, due to the confined configuration, the vibro-acoustic interaction is a strong two-way interaction and is modeled by coupling a flow-acoustic solver with a structural solver. The kinematic and dynamic continuity at the interface is ensured in this partitioned approach by a data exchange during runtime between the solvers. The data exchange is managed by the open-source coupling library preCICE [1]. The analysis of the flow-acoustic-structural interaction in a flexible flow duct with rectangular cross section was given in [2]. In this paper, the error resulting from the pressure mapping between both solvers is analyzed and an improved force mapping strategy is adopted.

1 INTRODUCTION

Lightweight flow ducts, nowadays used in for example ventilation and exhaust systems, have an inherent low mass-to-stiffness ratio. Therefore, they are very susceptible for structural vibrations caused by wall pressure fluctuations present in the confined turbulent airflow. This multi-physical interaction needs to be modeled sufficiently accurate for the design of effective solutions.

The wall pressure fluctuations consist of aerodynamic and acoustic contributions, which individual interactions with a flexible structure have been studied extensively in the past. This has led to (semi)-analytic descriptions of the aero-elastic interaction [3] and the vibro-acoustic interaction [4, 5, 6, 7] respectively. However, these do not suffice to describe the complex interaction between the confined aero-acoustic field and the structural dynamics of the duct walls [8, 9].

A more complete prediction of the aero-acoustic-structural interaction requires the modeling of the aerodynamic, acoustic and structural domains, as shown in Fig.1a. A monolithic solving approach would need to account for the large disparity in time and length scales characterizing the different physical domains, which would lead to a high computational cost. However, for the low Mach number applications targeted by this research, it is safe to assume that the acoustic and vibrational amplitudes remain small enough to not affect the aerodynamic domain, which leads to the simplified interactions visualized in Fig.1b. The aero-acoustic interaction can then be modeled with a hybrid flow-acoustic approach [10]

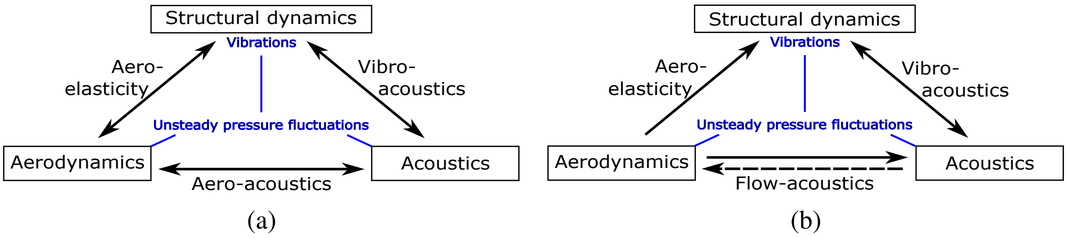

Figure 1: (a) Schematic overview of the multi-physical interactions present in a lightweight flow duct and (b) the simplified interaction scheme assumed for low Mach number applications.

and the aero-elastic interaction can be treated as a pressure load on the structural domain. The main modeling effort thus lies with the strong, two-way vibro-acoustic interaction.

As described in [2], a partitioned approach is adopted to model the vibro-acoustic interaction by coupling a flow-acoustic solver for the linearized Euler equations with a structural solver for linear elasto-dynamics. The coupling is facilitated by the communication and spatial mapping routines of the open-source library preCICE [1], making a data exchange during runtime possible. The main advantage of the partitioned approach is the freedom to retain the spatial and temporal discretization schemes optimal for each domain-specific solver.

In this paper an improvement of the spatial mapping strategy is presented. Section 2 starts with a description of the domain-specific solvers and the time domain coupling. Section 3 takes then a closer look at the possible spatial mapping strategies for this partitioned approach. The simulation case discussed extensively in [2], is re-used in section 4 to discuss the error related to the pressure mapping approach and the improved force mapping strategy. The conclusions are presented in section 5.

2 PARTITIONED SIMULATION APPROACH

The partitioned approach relies on domain-specific solvers and the data exchange between them. Therefore, this section will start with introducing the flow-acoustic solver and structural solver in subsections 2.1 and 2.2, respectively, although a more detailed description of each solver can be found in [2]. The data exchange between both solvers during runtime is explained in subsection 2.3.

2.1 Flow-acoustic solver

The flow-acoustic domain is modeled with the linearized Euler equations (LEE) in the time domain, for which an in-house solver has been developed [11, 12]. The matrix notation of the LEE for a three-dimensional cartesian domain can be expressed by use of the Einstein's summation convention, with x_r being one of the three cartesian coordinates $(x_1 = x, x_2 = y, x_3 = z)$:

$$\frac{\partial \underline{q}}{\partial t} + \frac{\partial \underline{F}_r}{\partial x_r} + \underline{\underline{C}}\,\underline{q} = 0 \tag{1}$$

The unknown first-order density fluctuations ρ, the velocity fluctuations u_r and the pressure fluctuations p are concatenated into the vector $\underline{q} = [\rho, \rho_0 u_1, \rho_0 u_2, \rho_0 u_3, p]^T$ with the subscript $\bullet_0$ denoting the mean flow quantity. The flux Jacobians in the r-direction are present in the matrix $\underline{F}_r = \underline{\underline{A}}_r \underline{q}$, and the effects of a non-uniform mean flow are modeled with the term $\underline{\underline{C}}\,\underline{q}$.

The spatial discretization of the LEE applies the nodal quadrature-free discontinuous Galerkin method over an unstructured straight-edge tetrahedral grid. Within each element, p^{th}-order Langrangian polynomials are used. Between neighbouring elements, a numerical Riemann flux solves the discontinuity.

A low-memory storage explicit fourth-order accurate Runge-Kutta scheme with eight stages carries out the time marching. The scheme uses optimized stage coefficients for the discontinuous Galerkin spatial discretization of the LEE [13].

2.2 Structural solver

The structural solver solves the governing equations of the Mindlin-Reissner shell theory [14], assuming the flexible duct walls are thin and made of a linear elastic material. The spatial discretization is performed with the finite element method using bilinear 2D quadrilateral elements in the commercial software SIEMENS SIMCENTER 3D 2019.2. The size of the obtained system matrices is reduced with the mode superposition method [14].

The reduced system of equations is integrated through time with an in-house solver implementing the Newmark-Beta algorithm [14]. The algorithm's coefficients are chosen such that the method is unconditionallly stable, has second-order accuracy, and adds no numerical dissipation [15]. This so-called constant-average-acceleration method is implicit, although the matrix inversion only needs to be computed once as long as the time step remains the same.

2.3 Time domain coupling

To include the effects of a strong two-way vibro-acoustic interaction, the flow-acoustic and structural solver must exchange data during runtime. This data exchange must ensure kinematic and dynamic continuity over the interface between both physical domains. The interface is in this case the flexible wall, which is implemented as a boundary condition of the flow-acoustic domain imposing the normal wall velocity $\underline{v}$, derived from the wall displacement $\underline{w}$ obtained by the structural solver. The pressure load exerted by the fluid on the wall, is implemented as a force load $\underline{F}$ on the structural domain. To allow a synchronized data exchange a common time step Δt must be defined, leaving the freedom for each solver to keep its own time step following its stability and accuracy rules and to subcycle until it reaches the common time step end.

To benefit from the combination of the explicit Runge-Kutta scheme and the implicit Newmark-Beta scheme, the data exchange follows the Conventional Serial Staggered scheme (CSS) [1]. The explicit scheme runs first as it requires the normal wall velocity data at the start of the common time step. The implicit scheme uses the force load data evaluated at the end of the common time step and therefore waits for the explicit scheme. The CSS scheme is illustrated in Fig.2, with the operator **RKDG** expressing the Runge-Kutta Discontinuous Galerkin discretization of the flow-acoustic domain and the operator **FENB** the Finite Element Newmark-Beta discretization of the structural domain:

$$\text{Flow-acoustic time step } \delta t_f : \ \mathbf{RKDG}(\underline{q}_t, \underline{v}_t) = \underline{q}_{t+\delta t_f} \Rightarrow \ \text{At end common time step } \Delta t : \ \underline{F}_{t+\Delta t} \tag{2}$$

$$\text{Structural time step } \delta t_s : \ \mathbf{FENB}(\underline{w}_t, \underline{F}_{t+\Delta t}) = \underline{w}_{t+\delta t_s} \Rightarrow \ \text{At end common time step } \Delta t : \ \underline{v}_{t+\Delta t} \tag{3}$$

For the interaction between a compressible fluid and a flexible structure, the CSS scheme is stable and converges to a monolithic method for a common time step size approaching zero [16]. The CSS scheme is managed by the preCICE library, which simplifies the implementation of the runtime data exchange to the linking of both solvers to preCICE and calling the appropriate routines.

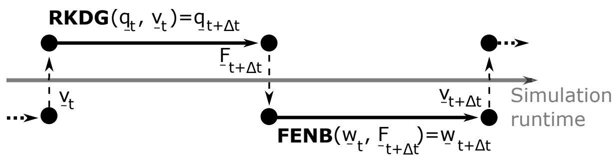

Figure 2: Illustration of the communication during runtime for one common time step Δt following the Conventional Serial Staggered scheme (CSS), assuming $\delta t_f = \delta t_s = \Delta t$. Adapted from [2] with permission of the American Institute of Aeronautics and Astronautics, Inc.

3 SPATIAL MAPPING STRATEGIES

Due to the different spatial discretization in each domain, a spatial mapping needs to take place to enable the data exchange between a source mesh and a target mesh. The data at the target mesh nodes is obtained by the multiplication of a mapping matrix with the source mesh data. Assuming small vibrational amplitudes, the mapping matrices are fixed, as the grids will not change during runtime. In subsection 3.1, the mapping matrix constraints are presented. Subsections 3.2 and 3.3 describe two possible mapping strategies, which will affect the accuracy of the partitioned simulation.

3.1 Mapping matrix constraints

Several approaches can be found in the literature for the calculation of the mapping matrix [1, 17]. In general, each mapping method can be assessed based on the trade-off between computational cost and accuracy. However, all methods need to adhere the mapping constraint imposed by the data to be mapped. Intensive variables, like pressure, need to be mapped consistently, which means that on each row of the mapping matrix the sum of the coefficients equals one. Extensive variables, like force, demand the conservative constraint for mapping, such that on each column the sum of the coefficients equals one.

3.2 Pressure mapping

In this work, the flow-acoustic domain is spatially discretized by a higher-order discontinuous method using tetrahedral elements. The boundary of this volumetric grid is formed by the triangular faces of the boundary tetrahedral elements. For the structural domain, the shell approximation simplifies the structural grid to a surface mesh, which is continuous and consists of bilinear quadrilateral elements. The length scales to be resolved typically require the flow-acoustic grid to be finer than the structural grid.

To handle the data exchange between the dense discontinuous higher-order mesh and the coarse continuous bilinear mesh, the choice was made in [2] to map pressures and velocities consistently over the interface. For the mapping method, the Nearest-Projection mapping algorithm offered by the preCICE library was taken as it has second-order accuracy. The mesh element shape needs to be communicated to preCICE, such that a linear interpolation between the element vertices can be determined. For a simplified 1D interface, the mapping is illustrated in Fig.3. As can be seen, only the data at the element vertices and not at the interior nodes of the high-order elements are taken into account, which means a loss of information. Another remark is that on the structural side the mapped pressures still need to be integrated to nodal forces. This can be done by multiplication with the non-dimensional mass matrix of the structural system, which comes down to a global bilinear integration.

3.3 Force mapping

To increase the accuracy order of the spatial integration, it is preferred to use the non-dimensional mass matrix of the flow-acoustic system, calculated from the higher-order shape functions. Therefore, an improvement of the mapping strategy is proposed where the integration is performed on the flow-acoustic side, mapping forces instead of pressure. Due to the discontinuous Galerkin formulation, the non-dimensional mass matrix is calculated for each triangular face on the interface, which means that the integration happens locally.

As force is an extensive variable, a conservative mapping method is necessary. This means that the global sum of the forces at all nodes needs to remain the same. Due to the local integration on each triangular face, the forces on each side of a discontinuous face edge need to be summed and not averaged. To get control of the mapping for further improvements, a radial search mapping routine [18] is implemented within the structural solver. Therefore, the flow-acoustic source mesh needs to be known by the structural solver, as well as the force data. For now, this is achieved by mapping each time step the nodal forces first 1-to-1 with the Nearest-Neighbor mapping of preCICE. In the future, this step will be omitted with a feature recently added to the preCICE library, namely *Direct Mesh Access*, which allows to communicate the data 'as is' from one solver to the other solver. Figure 4 shows the main ideas of the mapping strategy.

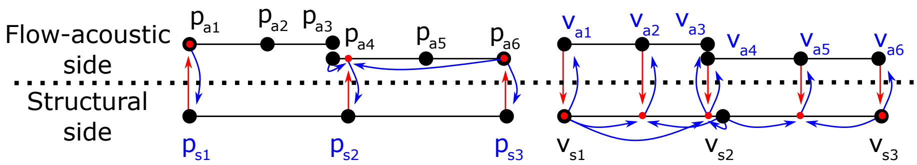

Figure 3: A simplified 1D interface, with on the flow-acoustic side two discontinuous elements of polynomial order 2. On the structural side there are two continuous structural elements. To illustrate the consistent Nearest-Projection mapping, red arrows show the orthogonal projection of the target mesh on the source mesh. The linear interpolation and data copy to the target mesh are shown with blue arrows. Adapted from [2] with permission of the American Institute of Aeronautics and Astronautics, Inc.

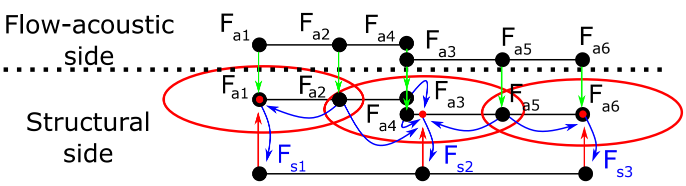

Figure 4: A simplified 1D interface, with on the flow-acoustic side two discontinuous elements of polynomial order 2. On the structural side there are two continuous structural elements. The green arrows show the 1-to-1 mapping. To illustrate the conservative radial search mapping, red arrows show the orthogonal projection of the structural nodes on the flow-acoustic source mesh. The data on the projected target mesh is determined by a weighted sum of the nodal forces within a certain distance, illustrated by the red ellips and the blue arrows. The weights are normalized to achieve conservation.

4 FLEXIBLE FLOW DUCT CASE

The flow-acoustic-structural interaction in a flexible flow duct with rectangular cross section was analyzed in [2]. In this work, the effect of the improved mapping strategy is shown for this case without flow. Subsection 4.1 discusses the geometry of the simulation case and subsection 4.2 the numerical parameters of the simulation. The results are discussed in subsection 4.3.

4.1 Case description

Figure 5 shows the flow duct system under consideration. It consists of a flexible duct segment of length L_z and two rigid duct segments. All duct segments have a rectangular cross section of inner dimensions L_x and L_y. Between the flexible duct segment and the rigid duct segments, a simply-supported connection is assumed. The used dimensions are given in Table 1, as well as the flexible wall material parameters, which are those for a thin steel sheet of thickness h. The ambient pressure p_0 and density ρ_0 of the fluid are respectively 101.325 kPa and 1.225 kg/m^3, which makes the speed of sound c_0 equal to 340.3 m/s.

As indicated in subsection 2.2, the mode superposition method is used to reduce the size of the system matrices of the structural model. For this, the mode shapes $\underline{\phi}_i$ and eigenfrequencies f_i are calculated for the structure *in vacuo*. To classify the mode shapes, a (m,n) index is used, with m indicating the circumferential mode type and n the axial mode type. The classification and eigenfrequency of the first 10 modes is given in Table 2 and Fig.6 shows the circumferential shape of these modes.

Table 1: Dimensions and material parameters of the flexible flow duct.

Length L_z	0.5 m	Inner cross section $L_x \times L_y$	0.2 m $\times$ 0.1 m
Young's modulus E	210 GPa	Density ρ_s	7800 kg/m^3
Thickness h	3 mm	Poisson's ratio ν	0.22

Table 2: Classification of the first 10 structural modes with their eigenfrequency f_i.

f_i [Hz] (m,n)	f_i [Hz] (m,n)	f_i [Hz] (m,n)
275.88 (1,1)	330.02 (2,1)	724.67 (3,1)
350.76 (1,2)	395.23 (2,2)	811.90(3,2)
483.93 (1,3)	515.65 (2,3)	
678.20 (1,4)	699.88 (2,4)	

4.2 Numerical set-up

The flow-acoustic grid is an unstructured tetrahedral grid with 31 345 elements, with characteristic lengths going from 25 mm in the rigid duct segments to 10 mm at the flexible walls. Choosing 5^{th}-order polynomial shape functions, this grid can resolve waves up to 8000 Hz according to the rule of thumb of [11]. The time step size is chosen as 1.47 µs, which should ensure stability of the time marching following the CFL rule [19]. A slip boundary condition is set at the rigid duct walls and a normal velocity boundary condition at the flexible duct walls. A non-reflecting boundary condition is imposed at the anechoic inlet and outlet.

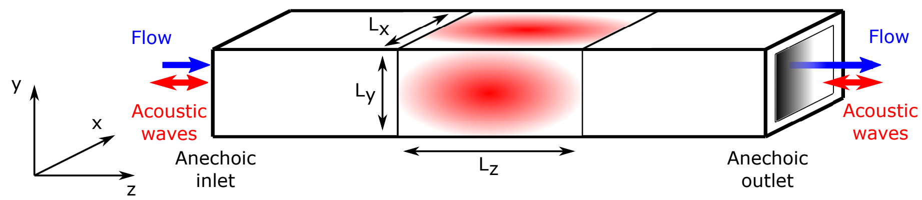

Figure 5: Illustration of the flow duct system, consisting of a rigid inlet flow duct, a flexible flow duct, and a rigid outlet flow duct. From [2]; reprinted by permission of the American Institute of Aeronautics and Astronautics, Inc.

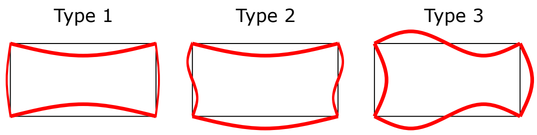

Figure 6: The first three circumferential mode types. Adapted from [2] with permission of the American Institute of Aeronautics and Astronautics, Inc.

The structural mesh should have at least 6 elements per free bending wavelength, therefore the used grid with 3000 quadrilateral elements of 10 mm characteristic size will be valid up to 5000 Hz. The simply-supported boundary condition represents the connection to the rigid duct walls. The modal basis consists of the first 100 modes, i.e. all modes with an eigenfrequency up to 4047.6 Hz. The modal damping ratio of each mode is set to 0.01. As the mode superposition method reduces the structural solver runtime, the same small time step as for the flow-acoustic solver is chosen without major impact on the overall computational cost. To establish a data exchange after every solver cycle, the common time step Δt is taken as 1.47 µs.

To exploit the capabilities of the time domain simulation, the system behavior is assessed over a broad frequency range by means of the impulse response technique [20]. In this work an acoustic pulse uniform over the cross section and with a Gaussian shape in the axial direction is injected at one of the non-reflecting boundaries. The propagation of the pulse and the system's response are then monitored at several positions in the rigid flow ducts.

For the analysis of the mapping strategy, no flow was taken into account. Also an analysis of the results of the impulse response technique are out of scope of present work. Therefore, the simulation is run only for approximately 0.015 s, saving at each time step the force and pressure values at all nodes lying on the bottom panel interface of the flexible flow duct.

4.3 Results

The spatial discretization of the flow-acoustic domain leads to 4804 triangular faces lying on the interface with the structural domain. Due to the higher-order discontinuous formulation, this means 100 884 nodes, of which 14 412 vertices. On the structural side, the full structural mesh lies on the interface, which gives 3060 nodes for the 3000 quadrilateral elements due to the bilinear continuous method.

As the consistent mapping of pressures was conceptually easier taking into account the higher-order discontinuous mesh, the results shown in [2] are generated with this approach. To get an idea of the force conservation of this mapping, the pressure field on the flow-acoustic side of the interface is locally integrated with the non-dimensional mass matrices of the flow-acoustic model. The pressure field on the structural side is integrated with the global non-dimensional mass matrix of the structural model. The sum of all forces on each side of the bottom panel interface is taken each time step and plotted in Fig.7a. The global error is determined as the sum on the structural side minus the sum on the flow-acoustic side and shown in Fig.7b. This shows quite a substantial error, proportional to the amplitude of the excitation.

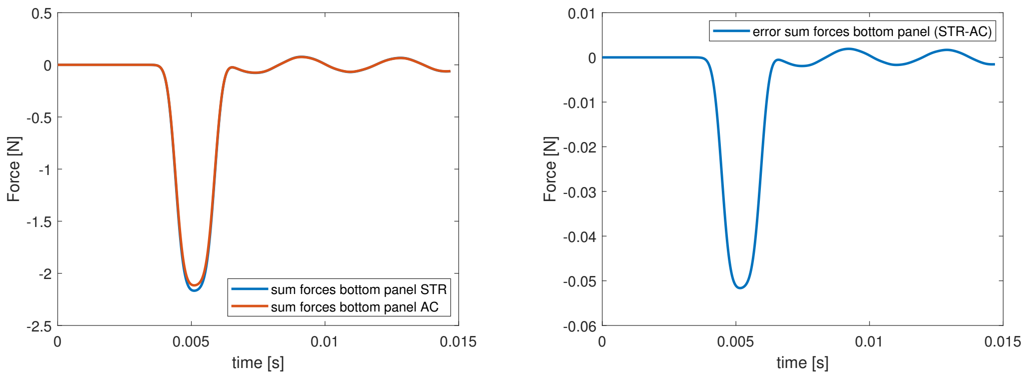

(a)

(b)

Figure 7: (a) The force sum over the bottom panel for the pressure mapping approach from the flow-acoustic source mesh (the AC curve) to the structural target mesh (the STR curve) and (b) the global error on the variable introduced by the mapping and the bilinear integration. The mapping matrix is calculated with the consistent Nearest-Projection method.

The summed forces over the bottom panel obtained with the improved force mapping strategy are shown in Fig.8a. As explained in subsection 3.3, this approach comes down to a double mapping: first the 1-to-1 mapping of the nodal forces from the flow-acoustic solver to the structural solver and then the conservative radial search mapping from the flow-acoustic source mesh to the structural target mesh. There is no difference visable in Fig.8a, but a small global error remains as shown in Fig.8b. Figure 9a shows that this error originates completely from the 1-to-1 mapping, due to the way the Nearest-Neigbor mapping handles the data at the discontinuities: it takes twice the value from the same node in the source mesh for both nodes on the discontinuity in the target mesh. By using the *Direct Mesh Access*-feature, recently added to the preCICE library, this error can be prevented in the future. The conservative mapping itself only introduces a negligible global error on the force sum, as expected by definition and as shown in Fig.9b. An important remark is that, although the data is conserved in a global way, local errors are still present. This will put an upper limit to the excitation of higher structural mode shapes.

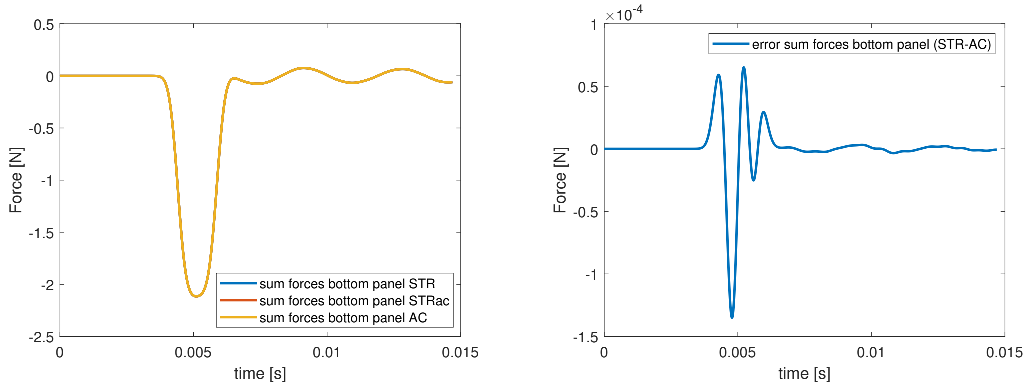

(a) (b)

Figure 8: (a) The force sum over the bottom panel for the force mapping approach and (b) the global error on the variable introduced by the mapping. The approach consists of a 1-to-1 mapping of the nodal forces from the flow-acoustic solver (the AC curve) to the structural solver (the STRac curve) and then the conservative radial search mapping from the flow-acoustic source mesh (the STRac curve) to the structural target mesh (the STR curve).

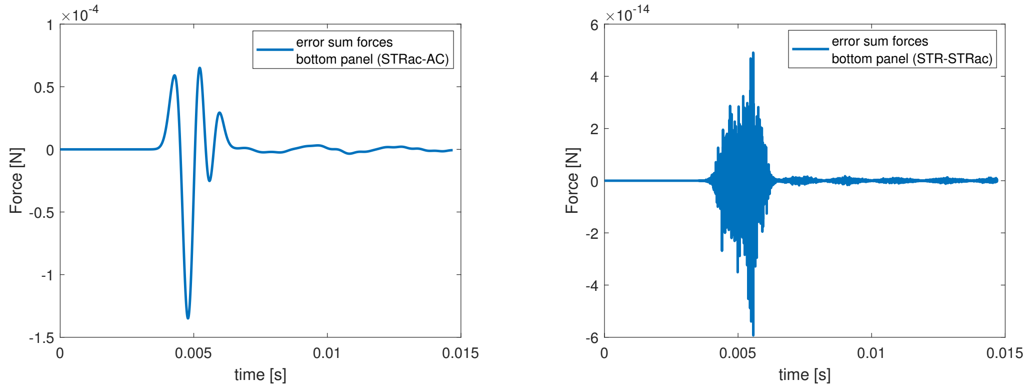

(a) (b)

Figure 9: (a) The global error of the force sum over the bottom panel for the 1-to-1 mapping of the nodal forces from the flow-acoustic solver (the AC curve) to the structural solver (the STRac curve) and (b) the global error of the force sum over the bottom panel for the conservative radial search mapping from the flow-acoustic source mesh (the STRac curve) to the structural target mesh (the STR curve).

5 CONCLUSIONS

This papers discusses the improved partitioned simulation approach for the flow-acoustic-structural interaction present in duct systems confining turbulent airflows at low Mach numbers. The flow-acoustic domain is solved by a higher-order Runge-Kutta Discontinuous Galerkin method for the linearized Euler equations. The structural domain is modeled with the linear elastic Mindlin-Reissner shell theory, discretized with a bilinear Finite Element Method and time-integrated with a Newmark-Beta algorithm.

The flow-acoustic-structural interaction exhibits a strong two-way vibro-acoustic interaction, which was included in the simulation by coupling both domain-specific solvers. The open-source coupling library preCICE [1] made this possible by facilitating a data exchange each time step. As an improvement to the pressure mapping approach used in [2], this paper presents a force mapping strategy. This force mapping strategy allows to conserve the data from the flow-acoustic solver in a global sense. Further research will need to check the error locally, which will form an upper limit to the excitation of higher structural mode shapes.

ACKNOWLEDGMENTS

The research of Jurgen Kersschot (fellowship no. 1SA6721N) is funded by a grant from the Research Foundation – Flanders (FWO). The Research Fund KU Leuven is gratefully acknowledged for its support.

REFERENCES

[1] H.-J. Bungartz, F. Lindner, B. Gatzhammer, M. Mehl, K. Scheufele, A. Shukaev, and B. Uekermann. preCICE–a fully parallel library for multi-physics surface coupling. *Computers & Fluids*, 141:250–258, 2016.

[2] J. Kersschot, H. Denayer, W. De Roeck, and W. Desmet. Simulation of the vibro-acoustic interaction in a flexible flow duct using a partitioned approach in the time domain. In *Proceedings of the AIAA AVIATION 2021 FORUM*, page 2148, 2021.

[3] M. K. Bull. Wall-pressure fluctuations beneath turbulent boundary layers: some reflections on forty years of research. *Journal of Sound and vibration*, 190(3):299–315, 1996.

[4] A. Cummings. Sound transmission through duct walls. *Journal of Sound and Vibration*, 239(4):731–765, 2001.

[5] N. Jade and B. Venkatesham. Experimental study of breakout noise characteristics of flexible rectangular duct. *Mechanical Systems and Signal Processing*, 108:156–172, 2018.

[6] L. Huang. A theoretical study of duct noise control by flexible panels. *Journal of the Acoustical Society of America*, 106(4):1801–1809, 1999.

[7] M. M. Sucheendran, D. J. Bodony, and P. H. Geubelle. Coupled structural-acoustic response of a duct-mounted elastic plate with grazing flow. *AIAA Journal*, 52(1):178–194, 2014.

[8] A. David, F. Hugues, N. Dauchez, and E. Perrey-Debain. Vibrational response of a rectangular duct of finite length excited by a turbulent internal flow. *Journal of Sound and Vibration*, 422:146–160, 2018.

[9] H. K. H. Fan, R. C. K. Leung, and G. C. Y. Lam. Numerical analysis of aeroacoustic-structural interaction of a flexible panel in uniform duct flow. *Journal of the Acoustical Society of America*, 137(6):3115–3126, 2015.

[10] W. De Roeck. *Hybrid methodologies for the computational aeroacoustics analysis of confined subsonic flows*. PhD thesis, KU Leuven, 2007.

[11] Y. Reymen. *3D High-Order Discontinuous Galerkin Methods for Time-Domain Simulation of Flow Noise Propagation*. PhD thesis, KU Leuven, 2008.

[12] T. Toulorge. *Efficient Runge-Kutta Discontinuous Galerkin Methods Applied to Aeroacoustics*. PhD thesis, KU Leuven, 2012.

[13] T. Toulorge and W. Desmet. Optimal Runge–Kutta schemes for discontinuous Galerkin space discretizations applied to wave propagation problems. *Journal of Computational Physics*, 231(4):2067–2091, 2012.

[14] M. A. Neto, A. Amaro, L. Roseiro, J. Cirne, and R. Leal. *Engineering computation of structures: the finite element method*. Springer, 2015.

[15] G. Noh and K.-J. Bathe. For direct time integrations: A comparison of the newmark and ρ_∞-bathe schemes. *Computers & Structures*, 225:106079, 2019.

[16] E. H. van Brummelen. Added mass effects of compressible and incompressible flows in fluid-structure interaction. *Journal of Applied mechanics*, 76(2):021206, 2009.

[17] A. de Boer, A. H. van Zuijlen, and H. Bijl. Comparison of conservative and consistent approaches for the coupling of non-matching meshes. *Computer Methods in Applied Mechanics and Engineering*, 197(49-50):4284–4297, 2008.

[18] P. Martinez Lera. *Modeling of Aerodynamic Noise Production and Flow-Acoustic Feedback for Wall-Bounded Low Mach Number Flows*. PhD thesis, KU Leuven, 2010.

[19] H. Wang, J. Yang, and M. Hornikx. Frequency-dependent transmission boundary condition in the acoustic time-domain nodal discontinuous galerkin model. *Applied Acoustics*, 164:107280, 2020.

[20] H. Denayer. *Flow-acoustic characterization of duct components using multi-port techniques*. PhD thesis, KU Leuven, 2017.